

## Regular article

A semi-empirical approach to the prediction of deformation behaviors of  $\beta$ -Ti alloysC.H. Wang<sup>a</sup>, A.M. Russell<sup>b</sup>, G.H. Cao<sup>a,\*</sup><sup>a</sup> State Key Laboratory of Advanced Special Steel and School of Materials Science and Engineering, Shanghai University, 149 Yanchang Road, Shanghai 200072, China<sup>b</sup> Department of Materials Science and Engineering, Iowa State University and Division of Materials Science and Engineering, Ames Laboratory of the U.S.D.O.E., Ames, IA 50011-2300, USA

## ARTICLE INFO

## Article history:

Received 2 July 2018

Received in revised form 19 August 2018

Accepted 19 August 2018

Available online xxxx

## Keywords:

Titanium alloys

Plastic deformation

Twinning

Stress-induced martensite

## ABSTRACT

A semi-empirical approach based on the compositional average electron-to-atom ratio ( $\bar{e}/\bar{a}$ ) and atomic radius difference ( $\bar{\Delta}r$ ) was proposed to refine the “d-electron method”. The  $\bar{e}/\bar{a}-\bar{\Delta}r$  diagram shows that Twinning/Stress-Induced Martensite (SIM) activates when  $\bar{\Delta}r > -2.5$ , and a low  $\bar{e}/\bar{a}$  or absolute value of  $\bar{\Delta}r$  favors Twinning/SIM by reducing the resistance of lattice shear. In addition to the phase stability, it suggests that the valence electron number and atomic radius of alloying element also determine the deformation mechanism in body-centered cubic Ti alloys. This alloy design method was verified by the tensile results of Ti-4Mo-4Co and Ti-6Mo-4Zr (at.%) alloys.

© 2018 Acta Materialia Inc. Published by Elsevier Ltd. All rights reserved.

Body-centered cubic ( $\beta$ ) Ti alloys have attracted increased attention due to their good hardenability, low elastic moduli, and shape memory properties [1,2].  $\beta$ -Ti alloys are defined as those Ti alloys with enough concentration of  $\beta$  stabilizing elements to retain 100% of the  $\beta$  phase at room temperature (RT) upon quenching from temperatures above  $\beta$  transus [3]. The mechanical properties of  $\beta$ -Ti alloys in a solution-treated condition have been reported to depend significantly on the deformation modes, such as stress-induced martensite (SIM), mechanical twinning, and dislocation slip [4]. The occurrence of martensitic transformation or mechanical twinning results in low yield strength and large uniform elongation through significant work hardening, while the dislocation slip induces high yield strength and poor uniform elongation [5]. The dominant deformation mechanism of  $\beta$ -Ti alloys evolves from martensitic transformation to mechanical twinning then to dislocation glide as the  $\beta$  phase stability increases [6]. Thus, altering the  $\beta$  phase stability by adding various  $\beta$ -stabilizing elements is one of the most common methods to design  $\beta$ -Ti alloys. The  $\beta$  phase stability of Ti alloys is commonly evaluated by the molybdenum equivalent ( $Mo_{eq}$ ), an equivalent concentration that combines the effects of the various  $\beta$ -stabilizing elements [3]. However, the  $Mo_{eq}$  is empirically based on binary systems and is problematic in multi-component systems due to the complex interactions among multiple elements [7].

A “d-electron method” has been proposed to reveal the relationship between plastic deformation behavior and  $\beta$  phase stability based on

two parameters,  $Bo$  and  $Md$  [8].  $Bo$ , the bond order, which measures the covalent bond strength between Ti and a particular alloying element, and  $Md$  being related to the metal d-orbital energy level, can be calculated based on the discrete-variational (DV)- $X\alpha$  cluster method [9]. The compositional averages of  $Bo$  and  $Md$  are denoted as  $\bar{Bo}$  and  $\bar{Md}$ , respectively. According to the “d-electron method”, a  $\bar{Bo}-\bar{Md}$  diagram was drawn to distinguish different phase zones [10], as shown in Fig. 1. In a sequence from the lower right to the upper left, the diagram is divided into  $\alpha$ ,  $\alpha + \beta$ , and  $\beta$  phase regions corresponding to the increase of  $\beta$  phase stability. A continuous Twinning/SIM region shows up beside the boundary of  $\beta$  and  $\alpha + \beta$  phases when the  $\bar{Bo}$  value is higher than 2.77, implying that deformation by Twinning/SIM requires a low  $\beta$  phase stability. Many  $\beta$ -Ti alloys with compositions located at the Twinning/SIM region were designed by the “d-electron method” and confirmed the formation of SIM and/or twins during deformation [11–13]. Nevertheless, there were also some reported mismatches between the locations in the  $\bar{Bo}-\bar{Md}$  diagram and the discovered deformation mechanisms. For example, the Ti-10V-3Fe-3Al (wt%) alloy lies within the twinning region, but in reality shows stress-induced  $\alpha'$  martensite in the microstructure after room temperature deformation [4]. Talling et al. [14] substituted Nb with V to produce a Ti alloy with the exact same  $\bar{Bo}$  and  $\bar{Md}$  of the original composition, however, the V-based alloy showed a contrasting deformation behavior comparing to the base one. Therefore, problems still exist in the use of the “d-electron method” and the  $\bar{Bo}-\bar{Md}$  diagram. Whether all the  $\beta$ -Ti alloys with a low  $\beta$  phase stability exhibit Twinning/SIM-dominant deformation behavior remains

\* Corresponding author.

E-mail address: [ghcao@shu.edu.cn](mailto:ghcao@shu.edu.cn) (G.H. Cao).

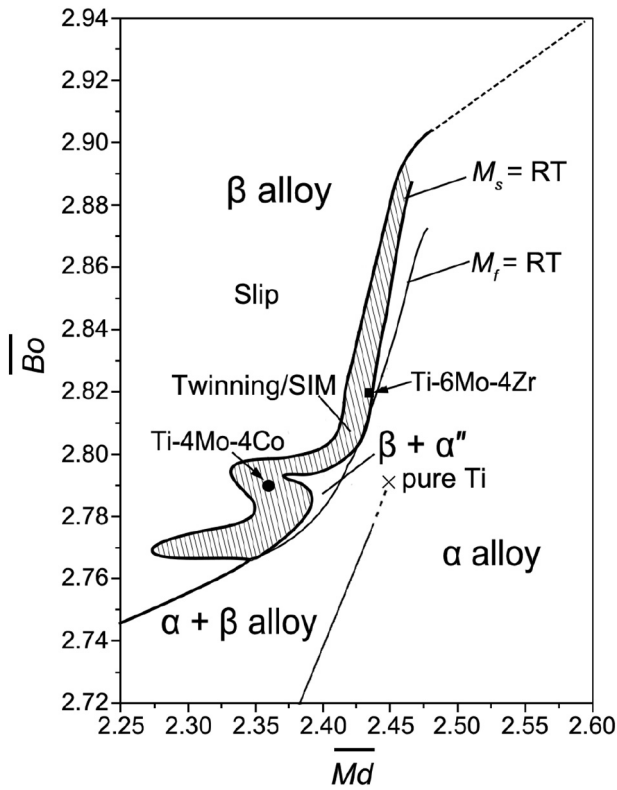


Fig. 1. The  $\overline{B}_0$ – $\overline{M}_d$  diagram showing that both Ti-4Mo-4Co and Ti-6Mo-4Zr alloys lie within the Twinning/SIM region.

unclear and needs to be investigated by more experimental and theoretical work.

In the present work, two  $\beta$ -type Ti-Mo-based alloys, Ti-4Mo-4Co and Ti-6Mo-4Zr (at.%) with compositions located within the Twinning/SIM region ( $\overline{B}_0 = 2.79$ ,  $\overline{M}_d = 2.36$  for Ti-4Mo-4Co, and  $\overline{B}_0 = 2.82$ ,  $\overline{M}_d = 2.44$  for Ti-6Mo-4Zr) were designed in order to achieve significant work hardening and superior ductility. However, the experimental results indicate the failure of the existing “d-electron method”. Thus, a new approach based on the average electron-to-atom ratio ( $\overline{e/a}$ ) and atomic radius difference ( $\overline{\Delta r}$ ) is proposed in this paper as a supplement to the “d-electron method”.

Ingots corresponding to the designed compositions were fabricated from 99.99% pure Ti, Mo, Co and Zr by levitation melting under an Ar atmosphere in a water-cooled Cu crucible. Subsequently, the ingots were cold-rolled to a thickness reduction of 70%. The cold-rolled sheets were sealed in quartz capsules evacuated to a pressure of  $\sim 1 \times 10^{-3}$  Pa and solution treated at 1273 K for 30 min followed by water quenching. The phase constitutions were determined by a D/MAX-3C X-ray diffractometer (XRD) using Cu  $K\alpha_1$  radiation ( $\lambda = 1.541$  Å). Tensile specimens with gauge dimensions of  $3 \times 1 \times 14$  mm were cut by electrical-discharge machining. Room temperature tensile tests were performed on a MTS C40 electronic universal testing machine with an Epsilon 3442 electronic extensometer at a cross-head speed of  $2 \times 10^{-3}$  mm  $s^{-1}$ .

The engineering stress-strain curves of the Ti-4Mo-4Co and Ti-6Mo-4Zr alloys tested at room temperature are shown in Fig. 2. As this figure shows, the two alloys exhibit distinctly different tensile properties and deformation behaviors. The Ti-6Mo-4Zr alloy displays a yield strength of 475 MPa, followed by extensive work hardening, resulting in a large tensile elongation of 28%. In contrast, the Ti-4Mo-4Co alloy shows a high yield strength of 980 MPa and a low ductility of 8% elongation, which are the characteristics of dislocation slip. Fig. 3 displays the XRD diffractograms of the Ti-4Mo-4Co and Ti-6Mo-4Zr alloys before and

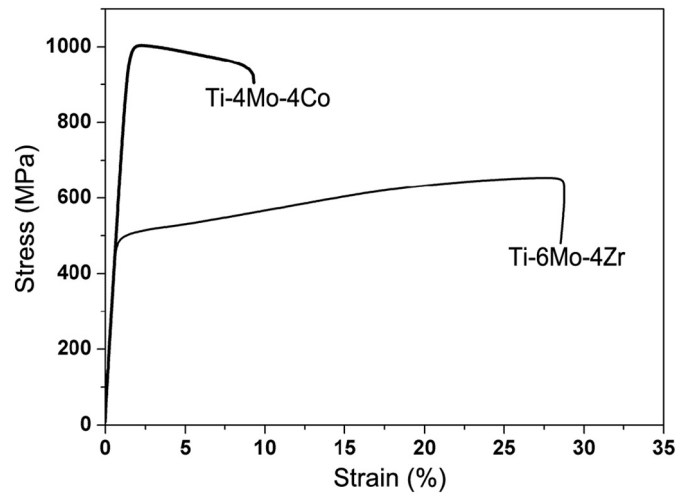


Fig. 2. Engineering tensile stress-strain curves of Ti-4Mo-4Co and Ti-6Mo-4Zr alloys.

after tensile deformation. Both alloys display single-phase  $\beta$  phase before tension. From the strongest (110)  $\beta$  peaks, the lattice parameters of  $\beta$  phases can be calculated to be  $a = 3.236$  Å for the Ti-4Mo-4Co alloy, and  $a = 3.265$  Å for the Ti-6Mo-4Zr alloy. No significant difference is observed in the XRD diffractogram of Ti-4Mo-4Co alloy after tensile testing. However, the XRD diffractogram of Ti-6Mo-4Zr alloy after tension shows the appearance of orthorhombic  $\alpha''$  martensite, which proves the formation of stress-induced  $\alpha''$  martensite during tension.

The tensile and XRD results reveal that the two alloys deform by different mechanisms, although both their compositions lie within the Twinning/SIM region of the  $\overline{B}_0$ – $\overline{M}_d$  diagram. The  $\overline{B}_0$ – $\overline{M}_d$  diagram fails to predict the deformation mechanism of Ti-4Mo-4Co alloy, which actually shows a slip-dominant behavior. The  $M_{0eq}$  of Ti-4Mo-4Co alloy is about 14, which is close to that of Ti-6Mo-4Zr alloy ( $M_{0eq} \approx 11$ ) considering the enhanced  $\beta$ -stabilizing effect of Mo by the addition of Zr [15]. Both alloys belong to the metastable  $\beta$ -Ti alloys ( $M_{0eq} \approx 8$ –24), suggesting that the different deformation behaviors may result from other influencing factors.

Martensitic transformations are diffusionless phase transformations characterized by a homogeneous shear of the parent lattice [16]. SIM transformation could be regarded as a special kind of martensitic reaction in which the driving force is an externally applied stress.

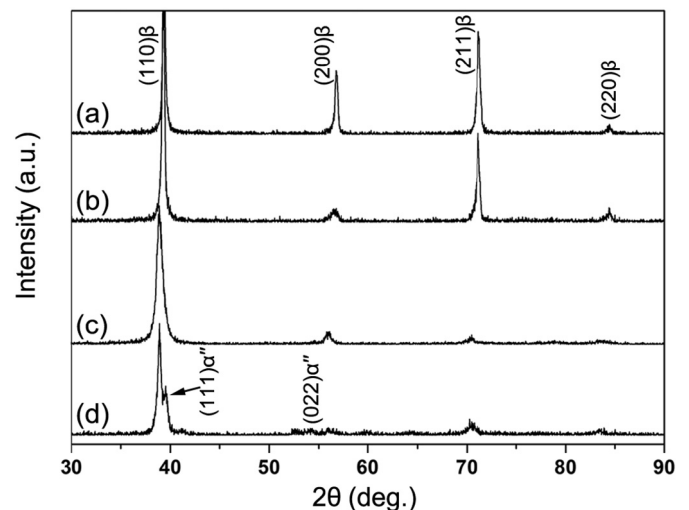


Fig. 3. XRD diffractograms of Ti-4Mo-4Co alloy (a) before and (b) after tension, and Ti-6Mo-4Zr alloy (c) before and (d) after tension.

Deformation twins form by a homogeneous simple shear of the parent lattice by highly coordinated individual atom displacements [17]. Both SIM and mechanical twinning need rigid shear of the parent lattice, in contrast to the chaotic processes of generation and growth of slip bands during deformation by dislocation glide. The shear modulus ( $c'$ ) is a measure of lattice shear stiffness, which represents the ability of the lattice to resist deformation at constant volume. Ikehata et al. [18] confirmed by first-principles calculations that the  $c'$  of a single-crystalline binary Ti alloy decreases with a decrease in the valence electron concentration. The  $\beta$  phase stability and mechanical properties of transition-metal binary Ti alloys were also closely related to the valence electron concentration [19]. The lattice shear stiffness increases with the increase of valence electron concentration in the range of 4–5.9. Moreover, the variation of unit-cell volume during alloying arising from the atomic size misfit between the Ti and alloying elements is an indicator of lattice strength of  $\beta$ -Ti alloys. The unit-cell volume and the binding energies between Ti and alloying atoms change with the relative concentration of the alloying atoms. The lower the binding energy, the stronger the bonds, and the more difficult the movement of atoms [20].

The use of semi-empirical parameters, such as valence electron concentration and atomic size difference, constitutes a basic contribution in the design of high entropy alloys (HEAs) and the prediction of intermetallic compounds [21,22]. Study of the effect of valence electron concentration on the phase stability in HEAs revealed that face-centered-cubic phases were stable at higher valence electron concentrations ( $\geq 8$ ) and body-centered-cubic phases were stable at lower valence electron concentrations ( $< 6.87$ ) [23]. Wang et al. [24] separated the solid solution, intermetallics, and metallic glass phases by calculating the atomic size difference. This paper tries to establish an approach to predict the deformation behaviors of  $\beta$ -Ti alloys by using two semi-empirical parameters. A compositional average of atomic radius difference between the matrix Ti and the alloying atoms ( $\overline{\Delta r}$ ) is used to estimate the misfit of atomic size, which can be expressed as:

$$\overline{\Delta r} = \sum_i^n c_i (r_i - r_{Ti}) \quad (1)$$

where  $n$  is the number of alloying elements,  $c_i$  is the atomic fraction of the  $i$ th atom,  $r_i$  is the atomic radius of the  $i$ th atom, and  $r_{Ti}$  is the atomic radius of Ti. Pauling's [25] experimental metallic radii of atoms were

used for the calculation of  $\overline{\Delta r}$ . The valence electron concentration can be defined as the compositional average of electron-to-atom ratio:

$$\overline{e/a} = \sum_i^n c_i e_i \quad (2)$$

where  $e_i$  is the valence number of the  $i$ th atom. The values of  $\overline{e/a}$  and  $\overline{\Delta r}$  of Ti-4Mo-4Co alloy are calculated to be 4.28 and  $-0.76 \text{ \AA}$ , while those of Ti-6Mo-4Zr alloy are 4.12 and  $0.35 \text{ \AA}$ , respectively. The numerical differences suggest that the contrasting deformation behaviors of Ti-4Mo-4Co and Ti-6Mo-4Zr alloys may be associated with  $\overline{e/a}$  and  $\overline{\Delta r}$ .

A diagram is drawn in Fig. 4 to explore the effects of  $\overline{e/a}$  and  $\overline{\Delta r}$  on the deformation mechanisms of Ti-4Mo-4Co, Ti-6Mo-4Zr, and other published  $\beta$ -Ti alloys. All the  $\beta$ -Ti alloys cited in Fig. 4 were solution treated before tested at room temperature [4–6,12–14,26–51]. Slip and Twinning/SIM regions were separated by dashed lines according to the compositions and deformation behaviors of referred studies. The following features can be summarized through locating the boundary between Slip and Twinning/SIM regions:

1. The slip region has a higher  $\overline{e/a}$  than that of the Twinning/SIM region, which mainly occurs when  $\overline{\Delta r} > -2.5$  and  $\overline{e/a} < 4.2$ .
2. The critical values for  $\overline{e/a}$  of the Twinning/SIM region have a peak when  $\overline{\Delta r}$  is close to 0, and then decline as the  $\overline{\Delta r}$  increases.

Deformation can only occur by slip to break the lattice completeness when the lattice is hard to shear. Instead, Twinning/SIM will be more easily activated. The increase of  $\overline{e/a}$  causes the increase of lattice shear stiffness, resulting in the deformation mechanism changes from Twinning/SIM to slip. Metallic solids can be regarded as assemblages of positive ions stabilized in positions surrounded by a sea of conduction electrons. The  $\overline{e/a}$  value represents the average quantity of electric charge of each positive ion, which is fixed by both the attracting and repelling Coulomb forces caused by the surrounding conduction electrons and neighboring positive ions. In an ideal body-centered cubic lattice, every position is equivalent, and every positive ion could be equivalent to the same one with an electric charge of  $\overline{e/a}$ . According to the Coulomb's law, the Coulomb force between two positive ions is directly proportional to the product of the charges and inversely proportional to the square of the interionic distance. The interionic distance is

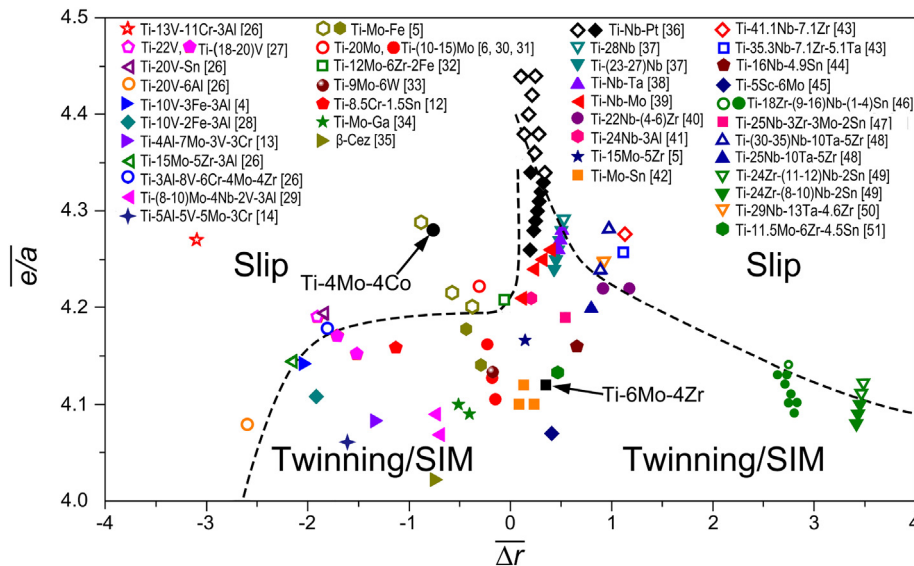


Fig. 4. The  $\overline{e/a}$ – $\overline{\Delta r}$  diagram in which the Twinning/SIM and Slip regions are distinguished according to the reviews of published works [4–6,12–14,26–51]. The use of empty and full bullets represents the Slip- and Twinning/SIM-dominated deformation mechanisms, respectively.

proportional to the lattice constant, which decreases with the decrease of average atomic radius (i.e.,  $\overline{\Delta r} + r_{Ti}$ ). Therefore, the Coulomb forces among metallic positive ions are proportional to the square of  $\overline{e/a}$  and increase with the decrease of  $\overline{\Delta r}$ . The increase of  $\overline{e/a}$  will cause a higher Coulomb force, namely, a higher bonding strength among atoms, and thereby induce a higher resistance against atomic movements and lattice shear. Therefore, the border value of  $\overline{e/a} = 4.2$  indicates the limit value of Coulomb forces that allows the atomic movements and lattice shear for Twinning/SIM occurring in most  $\beta$ -Ti lattices. The Coulomb forces and metallic bonding strength will get too high for lattice shear if  $\overline{e/a} > 4.2$ , by which the deformation can only proceed by dislocation slip.

Besides, the  $\beta$  phase stability improves as the  $\overline{e/a}$  ratio increases [52], inducing higher resistance for martensitic transformation. First principles calculations showed that the stacking fault energy of the  $\beta$  phase also increases with the increase of  $\overline{e/a}$ , and a low stacking fault energy is conducive for mechanical twinning [53]. Therefore, a low  $\overline{e/a}$  is favorable for both mechanical twinning and SIM.

According to Vegard's law [54], unit cell parameters should vary linearly with composition for a continuous substitutional solid solution in which atoms that substitute for each other are randomly distributed. The decrease of average atomic radius with compositional variation indicates the decrease of lattice constants and the shrinkage of lattice. The smaller the unit-cell volume, the stronger the binding force among the alloying atoms and the Ti atoms [20]. Thus, a small average atomic radius is disadvantageous to lattice shear. Consequently, mechanical twinning or SIM is suppressed when  $\overline{\Delta r} < -2.5$ .

In a substitutional solid solution such as  $\beta$ -Ti phase, atoms with different sizes have to occupy equivalent lattice positions, giving rise to intrinsic elastic energy due to atomic size misfit [55]. The increase of average size misfit between the matrix Ti and the alloying atoms (defined as the absolute value of  $\overline{\Delta r}$ ,  $|\overline{\Delta r}|$ ) generates higher elastic energy and stronger local lattice distortion [22]. As a result, the symmetry and regularity of the lattice decrease, making it harder for mechanical twinning and SIM to occur. Moreover, the solid solution strengthening is enhanced by increased size misfit and supplies a "mechanical" stabilization for the  $\beta$  phase. Thus, increasing  $|\overline{\Delta r}|$  results in an enhanced resistance against lattice shear and Twinning/SIM.

The combined effects of the aforementioned three factors account for the result that the region of Twinning/SIM is confined by  $\overline{\Delta r} > -2.5$  and  $\overline{e/a} < 4.2$ . Compared with the  $\overline{Bo}-\overline{Md}$  diagram, the  $\overline{e/a}-\overline{\Delta r}$  diagram reveals that  $\beta$ -Ti alloys with similar  $\beta$  stability may possess different abilities to deform by twinning or SIM. The valence electron number and atomic radius of alloying element should also be considered when designing  $\beta$ -Ti alloys. The locations of Ti-4Mo-4Co and Ti-6Mo-4Zr alloys in the  $\overline{e/a}-\overline{\Delta r}$  diagram match well with their deformation behaviors. Furthermore, considering the fact that  $r_{Nb} > r_{Ti} > r_{Mo} > r_{V}$ , the effect of  $\overline{\Delta r}$  may offer an approach to explain why most  $\beta$ -Ti shape memory alloys contain Nb.

In conclusion, two  $\beta$ -Ti alloys locating at the Twinning/SIM region of  $\overline{Bo}-\overline{Md}$  diagram showed distinctly different tensile properties. A semi-empirical approach based on the average electron-to-atom ratio ( $\overline{e/a}$ ) and atomic radius difference ( $\overline{\Delta r}$ ) was introduced to understand the deformation mechanisms of  $\beta$ -Ti alloys from this paper and formerly published work. In addition to the  $\beta$  phase stability,  $\overline{e/a}$  and  $\overline{\Delta r}$  also affect the deformation behaviors of  $\beta$ -Ti alloys by controlling the difficulty of lattice shear.  $\beta$ -Ti alloys with  $\overline{e/a}$  lower than 4.2 and  $\overline{\Delta r}$  larger than  $-2.5$  tend to deform by twinning or SIM rather than by dislocation slip.

## Acknowledgments

This work was supported by the Shanghai Committee of Science and Technology, China under Grant No. 16520721700.

## References

- [1] I. Weiss, S.L. Semiatin, *Mater. Sci. Eng. A* 243 (1998) 46–65.
- [2] M. Niinomi, M. Nakai, J. Hieda, *Acta Biomater.* 8 (2012) 3888–3903.
- [3] P.J. Bania, *JOM* 46 (1994) 16–19.
- [4] M. Ahmed, D. Wexler, G. Casillas, O.M. Ivasishin, E.V. Pereloma, *Acta Mater.* 84 (2015) 124–135.
- [5] X.H. Min, K. Tsuzaki, S. Emura, K. Tsuchiya, *Mater. Sci. Eng. A* 528 (2011) 4569–4578.
- [6] F. Sun, J.Y. Zhang, M. Marteleur, T. Gloriant, P. Vermaut, D. Laillé, P. Castany, C. Curfs, P.J. Jacques, F. Prima, *Acta Mater.* 61 (2013) 6406–6417.
- [7] Q. Wang, C. Dong, P.K. Liaw, *Metall. Mater. Trans. A* 46 (2015) 3440–3447.
- [8] M. Morinaga, N. Yukawa, T. Maya, K. Sone, H. Adachi, *Sixth World Conference on Titanium*, III, 1988 1601–1606.
- [9] M. Morinaga, N. Yukawa, H. Adachi, *ISIJ Int.* 72 (1986) 555–562.
- [10] D. Kuroda, M. Niinomi, M. Morinaga, Y. Kato, T. Yashiro, *Mater. Sci. Eng. A* 243 (1998) 244–249.
- [11] M. Abdel-Hady, K. Hinoshita, M. Morinaga, *Scr. Mater.* 55 (2006) 477–480.
- [12] C. Brozek, F. Sun, P. Vermaut, Y. Millet, A. Lenain, D. Embury, P.J. Jacques, F. Prima, *Scr. Mater.* 114 (2016) 60–64.
- [13] S. Sadeghpour, S.M. Abbasi, M. Morakabati, *J. Alloys Compd.* 650 (2015) 22–29.
- [14] R.J. Talling, R.J. Dashwood, M. Jackson, D. Dye, *Scr. Mater.* 60 (2009) 1000–1003.
- [15] X. Zhao, M. Niinomi, M. Nakai, T. Ishimoto, T. Nakano, *Mater. Sci. Eng. C* 31 (2011) 1436–1444.
- [16] E.R. Petty, *Martensite*, Longman, London, 1970.
- [17] J.W. Christian, S. Mahajan, *Prog. Mater. Sci.* 39 (1995) 1–157.
- [18] H. Ikehata, N. Nagasako, T. Furuta, A. Fukumoto, K. Miwa, T. Saito, *Phys. Rev. B* 70 (2004), 174113.
- [19] E.W. Collings, H.L. Gegel, *Scr. Metall.* 7 (1973) 437–444.
- [20] Y. Song, D.S. Xu, R. Yang, D. Li, W.T. Wu, Z.X. Guo, *Mater. Sci. Eng. A* 260 (1999) 269–274.
- [21] Z. Wang, Y. Huang, Y. Yang, J. Wang, C.T. Liu, *Scr. Mater.* 94 (2015) 28–31.
- [22] G.P. Tiwari, R.V. Ramanujan, *J. Mater. Sci.* 36 (2001) 271–283.
- [23] S. Guo, C. Ng, J. Lu, C.T. Liu, *J. Appl. Phys.* 109 (2011) 103505.
- [24] Z. Wang, W. Qiu, Y. Yang, C.T. Liu, *Intermetallics* 64 (2015) 63–69.
- [25] L. Pauling, *The Nature of the Chemical Bond and the Structure of Molecules and Crystals*, third ed. Cornell University Press, New York, 1960.
- [26] S. Hanada, O. Izumi, *Metall. Trans. A* 46 (1987) 265–271.
- [27] S. Hanada, O. Izumi, *Metall. Trans. A* 17 (1986) 1409–1420.
- [28] T.W. Duerig, J. Albrecht, D. Richter, P. Fischer, *Acta Metall.* 30 (1982) 2161–2172.
- [29] L.C. Zhang, T. Zhou, S.P. Alpay, M. Aindow, M.H. Wu, *Appl. Phys. Lett.* 87 (2005) 241909.
- [30] C.H. Wang, C.D. Yang, M. Liu, X. Li, P.F. Hu, A.M. Russell, G.H. Cao, *J. Mater. Sci.* 51 (2016) 6886–6896.
- [31] C.H. Wang, M. Liu, P.F. Hu, J.C. Peng, J.A. Wang, Z.M. Ren, G.H. Cao, *J. Alloys Compd.* 720 (2017) 488–496.
- [32] K.K. Wang, L.J. Gustavson, J.H. Dumbleton, *Beta Titanium Alloys in 1990's*, TMS of AIME 1993, pp. 49–60.
- [33] F. Sun, J.Y. Zhang, M. Marteleur, C. Brozek, E.F. Rauch, M. Veron, P. Vermaut, P.J. Jacques, F. Prima, *Scr. Mater.* 94 (2015) 17–20.
- [34] H.Y. Kim, Y. Ohmatsu, J.I. Kim, H. Hosoda, S. Miyazaki, *Mater. Trans.* 45 (2004) 1090–1095.
- [35] T. Grosdidier, C. Roubaud, M.J. Philippe, Y. Combres, *Scr. Mater.* 36 (1997) 21–28.
- [36] H.Y. Kim, N. Oshika, J.I. Kim, T. Inamura, H. Hosoda, S. Miyazaki, *Mater. Trans.* 48 (2007) 400–406.
- [37] H.Y. Kim, H. Satoru, J.I. Kim, H. Hosoda, S. Miyazaki, *Mater. Trans.* 45 (2004) 2443–2448.
- [38] H.Y. Kim, S. Hashimoto, J.I. Kim, T. Inamura, H. Hosoda, S. Miyazaki, *Mater. Sci. Eng. A* 417 (2006) 120–128.
- [39] Y. Al-Zain, H.Y. Kim, T. Koyano, H. Hosoda, T.H. Nam, S. Miyazaki, *Acta Mater.* 59 (2011) 1464–1473.
- [40] J.I. Kim, H.Y. Kim, T. Inamura, H. Hosoda, S. Miyazaki, *Mater. Sci. Eng. A* 403 (2005) 334–339.
- [41] Y. Fukui, T. Inamura, H. Hosoda, K. Wakashima, S. Miyazaki, *Mater. Trans.* 45 (2004) 1077–1082.
- [42] T. Maeshima, S. Ushimaru, K. Yamauchi, M. Nishida, *Mater. Trans.* 47 (2006) 513–517.
- [43] L.M. Elias, S.G. Schneider, S. Schneider, H.M. Silva, F. Malvisi, *Mater. Sci. Eng. A* 432 (2006) 108–112.
- [44] E. Takahashi, T. Sakurai, S. Watanabe, N. Masahashi, S. Hanada, *Mater. Trans.* 43 (2002) 2978–2983.
- [45] T. Maeshima, M. Nishida, *Mater. Trans.* 45 (2004) 1101–1105.
- [46] J. Fu, A. Yamamoto, H.Y. Kim, H. Hosoda, S. Miyazaki, *Acta Biomater.* 17 (2015) 56–67.
- [47] H. Zhan, W. Zeng, G. Wang, D. Kent, M. Dargusch, *Scr. Mater.* 107 (2015) 34–37.
- [48] N. Sakaguchi, M. Niinomi, T. Akahori, J. Takeda, H. Toda, *Mater. Sci. Eng. C* 25 (2005) 363–369.
- [49] L.L. Pavón, H.Y. Kim, H. Hosoda, S. Miyazaki, *Scr. Mater.* 95 (2015) 46–49.
- [50] Q. Li, M. Niinomi, J. Hieda, M. Nakai, K. Cho, *Acta Biomater.* 9 (2013) 8027–8035.
- [51] J.A. Feeney, M.J. Blackburn, *Metall. Trans.* 1 (1970) 3309–3323.
- [52] P. Laheurte, F. Prima, A. Eberhardt, T. Gloriant, M. Wary, E. Patoor, *J. Mech. Behav. Biomed. Mater.* 3 (2010) 565–573.
- [53] Y. Yang, G.P. Li, H. Wang, Q. Wu, L.C. Zhang, Y.L. Li, K. Yang, *Scr. Mater.* 66 (2012) 211–214.
- [54] L. Vegard, *Z. Phys.* 5 (1921) 17–26.
- [55] W.T. Geng, A.J. Freeman, G.B. Olson, *Phys. Rev. B* 63 (2001) 165415.